Mathematical Biosciences and Engineering

MBE, 20(1): 975–997.
DOI: 10.3934/mbe.2023045
Received: 11 July 2022
Revised: 28 September 2022
Accepted: 03 October 2022
Published: 21 October 2022

http://www.aimspress.com/journal/MBE

*Research article*

# Applied machine learning for blood pressure estimation using a small, real-world electrocardiogram and photoplethysmogram dataset

**Mark Kei Fong Wong[1], Hao Hei[2], Si Zhou Lim[1] and Eddie Yin-Kwee Ng[1,*]**

[1] School of Mechanical and Aerospace Engineering, Nanyang Technological University, 639798, Singapore
[2] School of Electrical and Electronic Engineering, Nanyang Technological University, 639798, Singapore

* **Correspondence:** Email: myknng@ntu.edu.sg.

**Abstract:** Applying machine learning techniques to electrocardiography and photoplethysmography signals and their multivariate-derived waveforms is an ongoing effort to estimate non-occlusive blood pressure. Unfortunately, real ambulatory electrocardiography and photoplethysmography waveforms are inevitably affected by motion and noise artifacts, so established machine learning architectures perform poorly when trained on data of the Multiparameter Intelligent Monitoring in Intensive Care II type, a publicly available ICU database. Our study addresses this problem by applying four well-established machine learning methods, i.e., random forest regression, support vector regression, Adaboost regression and artificial neural networks, to a small, self-sampled electrocardiography-photoplethysmography dataset (n = 54) to improve the robustness of machine learning to real-world BP estimates. We evaluated the performance using a selection of optimal feature morphologies of waveforms by using pulse arrival time, morphological and frequency photoplethysmography parameters and heart rate variability as characterization data. On the basis of the root mean square error and mean absolute error, our study showed that support vector regression gave the best performance for blood pressure estimation from noisy data, achieving an mean absolute error of 6.97 mmHg, which meets the level C criteria set by the British Hypertension Society. We demonstrate that ambulatory electrocardiography- photoplethysmography signals acquired by mobile discrete devices can be used to estimate blood pressure.

**Keywords:** non-occluding blood pressure; noisy data; machine learning; photoplethysmography; electrocardiography

## 1. Introduction

Elevated blood pressure (BP) is known as hypertension, and it is a major healthcare burden as a major contributor to cardiovascular disease [1]; it is also a leading cause of heart disease and stroke [2,3]. Hypertension is a silent killer that can silently damage a person's body for years before symptoms appear. Uncontrolled high BP can lead to disability, a poor quality of life or even a fatal stroke or heart attack. Regular and frequent measurement of BP is essential for management of the condition and to ensure that appropriate therapeutic measures are taken to reduce the risk of life-threatening complications.

A systolic blood pressure (SBP) greater than 140 mmHg and a diastolic blood pressure (DBP) greater than 90 mmHg is termed hypertension [4]. In the traditional brachial cuff method of measuring BP, a cuff is applied to the arm to block blood flow in the brachial artery, whereas a variation of the auscultatory method or oscillometric method is used to derive SBP and DBP. However, in the continuous measurement of BP, the repeated squeezing of the upper arm by the cuff is uncomfortable for the subject, so the conventional brachial cuff method for ambulatory BP monitoring has low compliance.

There is an ongoing clinical need for less invasive methods for continuous measurement of BP. Continuous measurement of BP without a cuff is an ongoing medical and scientific endeavor [5,6].

### *1.1. Background of electrocardiography-photoplethysmography based BP estimation*

Among the many methods developed for non-occlusive BP monitoring, electrocardiography (ECG)-and photoplethysmography (PPG)-based techniques have been studied extensively because of the relatively unobtrusive acquisition of ECG and PPG signals in a single individual [7–9]. In the clinic, ECG is the gold standard for diagnosing cardiovascular electrical activity.

A single-lead ECG can be recorded in a person with two electrodes placed laterally over the heart. ECG acquisition is versatile and can be performed with wet Ag-AgCl electrodes on the skin or with the dry metal contacts of a wearable. The PPG signal, on the other hand, is a hemodynamic bio-optical measurement of blood volume obtained from the attenuation of transmitted or reflected light due to the spectral absorption of pulsatile blood flow in the region. PPG signals are usually acquired at an extremity, such as the fingertip [10] or wrist, and they are an important waveform for pulse oximetry and numerous other patient monitoring metrics [11,12].

The electrical activity of the heart produces the characteristic ECG waveform in which the QRS peak indicates contractile activity of the ventricle. This is called systole, and blood is pumped out of the heart into the vascular system. When the blood pulse reaches the extremity where the PPG sensor is located, the attenuation of the light produces the characteristic PPG waveform.

When measured simultaneously, the time difference between the peak of the QRS wave and the systolic peak of the PPG waveform is known as the pulse arrival time (PAT). Figure 1 represents a coalesced sampling of 30 seconds of ECG and PPG signals with identified ECG and PPG pulse peaks from an individual that was used to determine the PAT.

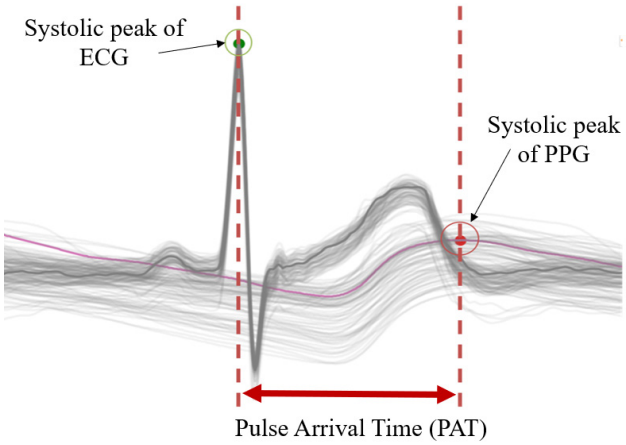


**Figure 1.** When ECG and PPG signals are synchronized for 30 seconds, the result is a mean-value PAT, as indicated by the time difference between the R peak of the ECG and the systolic peak of the corresponding PPG.

The relationship between PAT and BP has been evidenced by independent researchers [13–16], and the ECG-PPG approach has permitted a feasible way to determine non-occlusive BP due to the relative ease and non-invasiveness of acquiring ECG and PPG signals from an individual.

However, the parameter PAT alone is inadequate as a linear relationship to BP [17], in part because of the complex non-Newtonian hemorheological behavior of blood [18], the viscoelastic properties of blood vessels [19–23], i.e., they flex and contract with each heartbeat [24] and the fact that the inclusion of the pre-ejection period (PEP) adds an indeterminate variable [25]. The arterial distensibility or stiffness resists the pressure exerted on the vessel walls by the pulsatile, circulating blood. The nonlinear hemodynamic properties of the cardiovascular network and the viscoelastic properties of blood [26] contribute directly to the effects on BP.

Although the hemomechanical effects of arterial properties on BP are well known, the physiological influence on the beat-to-beat relationship BP is largely averaged and reduced in significance so that, by applying machine learning or deep learning to ECG-PPG and its constituent morphologies, BP can be estimated with a reasonable degree of high accuracy [27–36].

The recent popularity of smartwatches and fitness trackers with bio-monitoring capabilities has also enabled a convenient way for the biosignals to be obtained in daily life [37,38], thereby reinforcing the direction of BP monitoring with ECG-PPG machine learning approaches.

Thus, it is important to acknowledge that just the PAT and feature extraction of pulse morphologies alone will not yield clinically acceptable BP values, and that further work is required for acceptance of machine learning-based BP estimation in a healthcare environment.

### *1.2. Limitations of machine learning/deep learnings on ECG-PPG approaches*

Conventional machine learnings and unsupervised deep learning approaches applied to feature sets extracted from ECG and PPG signals to predict BP are well established in literature [29,31–35]. Despite the various machine learning models and techniques proposed, the majority of the current research relies on large publicly available datasets such as the Multi-Parameter Intelligent Monitoring in

Intensive Care (MIMIC-II) [39] or PhysioNet datasets [40], which are acquired from intensive care unit (ICU) patient monitors and include the required ECG, PPG and BP data, among others.

From the same dataset, the application of different machine learning approaches leads to different results [41]. The best-performing recent studies almost always implemented deep learning [34,35]. Recent studies using convolutional neural networks (CNNs) with long short-term memory (CNN-LSTM) [42], repetitive neural networks with long-short term memory (LSTM) [43] and artificial neural networks (ANNs) with LSTM [8] achieved very accurate predictions, with mean absolute differences of less than 2 mmHg.

Although the performance is impressive, the calculation was based on "clean" ECG and PPG waveforms from a patient monitor in the ICU, where patients are often immobile or unconscious; hence, the long time series recorded are not affected by motion artifacts. While this is advantageous for LSTM-type deep learnings, which are best suited for longitudinal and time-series data, this is not the case in a real-world setting where input datasets from wearables may contain short sporadic sequences recorded for each subject, as LSTM and any time-series analysis approach perform poorly on disjointed or sporadic data. Table 1 summarizes the drawbacks of the deep learning methods in a real-world setting.

**Table 1.** Disadvantages of unsupervised deep learning models in real-world BP estimation.

| Too "clean" | Too "slow" |
|---|---|
| • The datasets are almost always acquired from "clean" clinical sources or patient monitors, where biosignals are free of motion and other corrupting artifacts.<br>• Unsupervised neural networks with "black-box" architectures will face challenges in acquiring necessary regulatory approval, even in the De-Novo regulatory pathway with the Food and Drug Administration (FDA), due to low explainability of the model | • The neural network models are heavily dependent and require training from a large dataset that researchers acquire from large-domain open-source databases such as MIMIC-II or PhysioNet.<br>• The neural networks are extremely computationally intensive, often requiring high-performance computing; thus, they are unsuitable when battery life is limited. |

In CNNs, the main problem is that the neural network architecture is a black box, which translates into low explainability. As more layers are added, the network becomes more complex, and it becomes increasingly difficult to understand how and why the deep learning model produces a particular estimate. Since the regression task is a healthcare domain that potentially supports medical decisions, low explainability is not desirable, despite the low mean absolute error (MAE). For this reason, explanatory power is often overlooked as an important factor when evaluating and selecting machine learning models. In addition, convolutional-type neural networks have high computational costs and may not be suitable for edge computing or wearable applications where battery power availability is limited.

Despite reports of the superiority of deep learning methods over traditional machine learning approaches in estimating BP from ECG-PPG data obtained from MIMIC-II, the same techniques

perform far worse than traditional machine learnings on small datasets or signals obtained from mobile ambulatory subjects.

When signals are acquired from real biomonitoring devices or smart wearables, ECG/PPG waveforms are often corrupted by motion and noise artifacts. There is an urgent need to resort to supervised machine learning methods whose architecture and solution results are predictable, repeatable and flexible enough to be trained with a smaller dataset. Although many efforts have been made to suppress these artifacts, the elimination of random noise remains a very difficult task. Relying on clinically acquired signals from biomedical databases is not representative of real signals that are affected by artifacts.

While simple models are preferred to fit small datasets, linear regression and other very simple machine learning models are also inappropriate because they are generally unable to detect the nonlinear relationship between PPG morphological features and BP. This is critical for estimating BP because the morphological PPG features make up the largest portion of the feature set, and failure to identify the relationship can result in these features being redundant or even negatively impacting performance.

In this work, a small dataset of 54 subjects with imperfect ECG and PPG waveforms was self-selected and a corresponding BP was recorded and trained. The goal was to compare different machine learning models and develop an optimal approach for BP estimation, including preprocessing, feature extraction, feature selection, an optimal machine learning model and hyperparameter tuning.

Although the dataset is relatively small, more features were selected to compensate for this (24 features), which allowed slightly more complex models, such as support vector regression (SVR) and artificial neural network (ANN) models with a hidden layer.

To the best of our knowledge, few studies have intentionally applied training to a dataset with imperfect biosignal waveforms that are more consistent and representative of real-world conditions. When the PPG waveform is acquired, it contains numerous morphologies that are poorly discernible and not automatically flagged for the reference points to be identified; these essentially constitute artifact-like noise that could result from minute movements caused by the subject's breathing when the finger is placed on the PPG sensor.

Finger pressure on the sensor causes amplitude and baseline changes that can be observed throughout the data acquisition. This is a key difference between a self-collected dataset and a clinically acquired "clean" dataset from databases such as MIMIC-II. Because the models from machine learning recognize patterns from the training dataset and make the final prediction based on the learned patterns, using imperfect waveforms as the training dataset can lead to more robust prediction even when noise and motion artifacts are present in the input signals.

## 2. Materials and methods

### *2.1. ECG-PPG acquisition device*

The Maxim Integrated MAX86150 chip was used for the implementation of PPG and ECG because the solution had built-in discrete LED drivers, an internal LED illuminator, an embedded photodiode sensor and specific discrete transimpedance op-amp filters with ambient light rejection and amplifiers with programmable gain Analog to Digital Converter and an ECG analog front-end. It is a ready-to-use reflectance-type complete heart rate monitor and SpO2 biopotential measurement

solution capable of synchronized PPG and ECG measurements with digital $I^2C$ output directly to an ARM Cortex-M4 microcontroller (Maxim MAX32630); the team also built a protective enclosure around the electronics to guide the participant's finger onto the PPG sensor (see Figure 2).

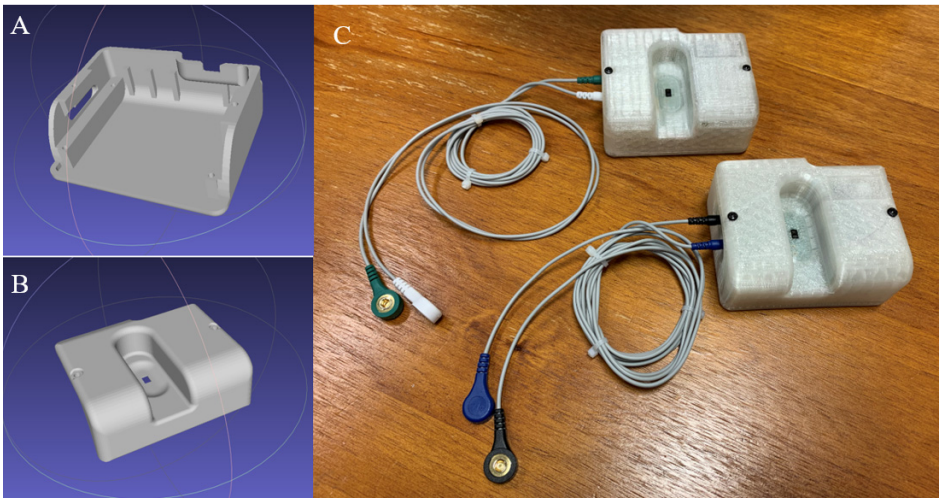


**Figure 2.** Labels A and B respectively show the top and bottom sections of the custom-designed protective enclosure for the electronics that was rapidly prototyped via additive manufacturing. C: Two prototype ECG-PPG data loggers completed for implementation in the study; the ECG wires were connected to wet electrodes when a study was conducted.

The MAX86150 has low power consumption, which makes it suitable for battery-powered wearables, as well as a common mode rejection ratio of 136 dB; and, the ECG analog front-end can operate on dry electrode impedances without the need for a third electrode (right-leg drive). The device was built to stream data directly via Bluetooth to a Windows 10 laptop where they were recorded on a GUI script written in Python language.

### *2.2. Signal acquisition*

The dataset collected consisted of information from 54 volunteer individuals (35 male, 19 female, aged 21–57 years); the ECG, PPG and BP data were recorded simultaneously for each person.

A commercially available BP monitor (Omron Hem-7600T) attached to the participant's left upper arm was used for BP measurement, while ECG and PPG signals were obtained from MAX86150#VSYS software v2.4.01 by placing the participant's left index fingertip on a single PPG sensor and attaching two wet ECG electrodes to both wrists of the participant for ECG measurement (see Figure 3); ECG and PPG signals were recorded simultaneously for about 3 minutes at a sampling rate of 400 Hz, while the measurement of BP was repeated three times during the 3 minutes with a 1-minute rest interval to allow blood to re-pool at the extremity after occlusion; for an individual with no cardiovascular history of stenosis or regurgitation, the PPG waveform was observed to return to expected amplitudes after several heartbeats. Table 2 describes the data acquisition protocol.

The Omron BP was activated three times, i.e., at the beginning of the measurement, in the middle of the measurement and after the measurement, resulting in three sets of SBP and DBP for each

participant. Since BP is influenced by posture [44], all participants adopted a sitting position during the 5 minutes of measurement to maintain the consistency of data collection. A total of 3 minutes of ECG-PPG recordings were then acquired for analysis.

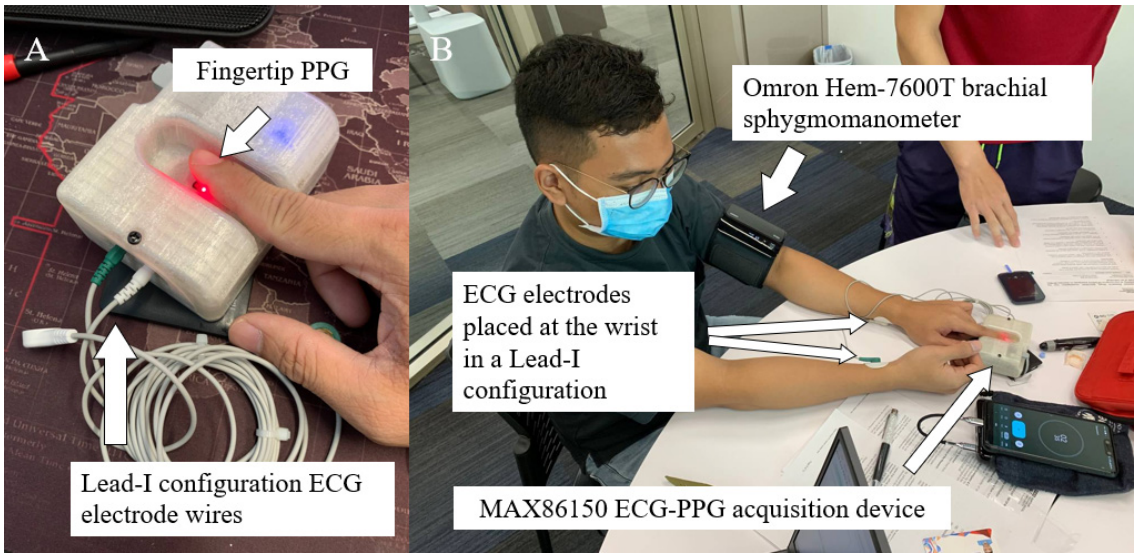


**Figure 3.** A: Close up of the enclosed MAX86150-based ECG-PPG capture device designed by the authors; active operation of the device with a user's finger on the device finger sensor window can be seen with the red LED illuminated. B: Typical seated posture during signal acquisition; white arrows denote the positions on electrodes and brachial sphygmomanometer on the participant's left arm.

**Table 2.** Data acquisition protocol.

| Time | Activity |
|---|---|
| $0^{th}$ minute | $1^{st}$ BP reading taken with the Omron HEM-7600T and takes ~20 seconds |
| $1^{st}$ minute | ECG-PPG recording for 1 minute |
| $2^{nd}$ minute | 2nd BP reading taken |
| $3^{rd}$ – $4^{th}$ minute | ECG-PPG recording for 2 minutes |
| $5^{th}$ minute | 3rd BP reading taken |

### *2.3. Signal processing*

The raw signals or ECG and PPG signals recorded for each participant were susceptible to many external factors, such as the pressure applied by the index finger on the PPG sensor and noise [45]. Since this work was aimed to work on "imperfect" waveforms, only some simple but necessary data cleaning was performed.

The extent of data cleaning was such that feature extraction, e.g., peak detection, could be performed without major problems, e.g., double peaks in a single waveform. This step of finding the balance is critical to the accuracy and reliability of the results from machine learning. Although this work is based entirely on the self-collected small imperfect waveforms that correspond to the real

scenario, if the basic features of these signals (peaks and troughs) were not correctly identified, the machine learning models would learn illogical inputs, which would inevitably lead to poor performance.

Given this trade-off, the data cleaning presented in this paper was simplified while still allowing sufficiently good identification of the features of biosignals, unlike many other studies that focused exclusively on achieving de-noised or artifact-suppressed waveforms. Figure 4 represents the stages of signal processing implemented upon acquisition of ECG-PPG signals.

Upon signal acquisition, the ECG and PPG signals were MIN-MAX normalized so that they all had precisely the same scale and differences in scale. A simple illustration of PPG preprocessing is shown in Figure 5.

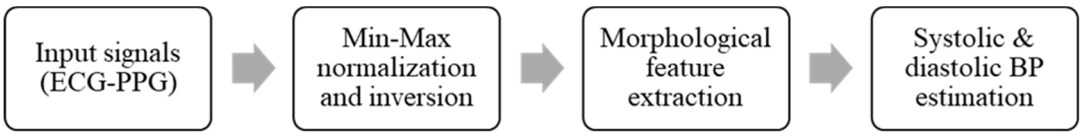


**Figure 4.** Simplified overview of the signal processing stages in this work.

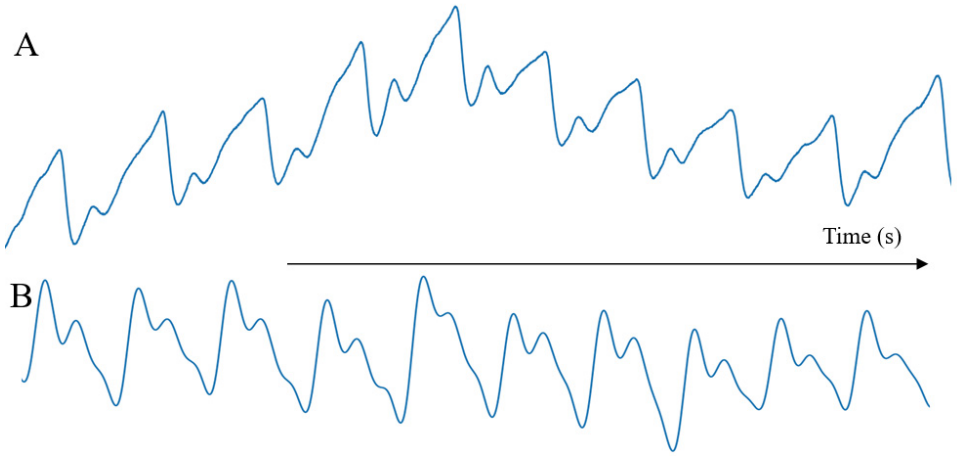


**Figure 5.** A: Raw PPG, and B: filtered and processed PPG that has been normalized and inverted to reflect the correct morphological representation; 10 heartbeats are represented, the amplitude values of which were normalized across the entire bandwidth of the recording in the Y axis, so they are unitless for visualization.

Since the MAX86150 is a reflectance-type PPG sensor that captures attenuated reflected light, the normalized PPG signals would need to be inverted for accurate morphological representation. The normalized and inverted PPG signals were then further processed to capture the first and second derivatives, i.e., the photoplethysmography velocity (VPG) and photoplethysmography acceleration (APG) signals to be obtained [10]. ECG, PPG, VPG and APG data were then applied to the filters listed in Table 3 for waveform smoothing and high-frequency noise removal.

**Table 3.** Selected cut-off frequencies.

| Signal | Filter | Cutoff (Hz) |
|---|---|---|
| ECG | $5^{th}$ order Low pass | 20 |
| PPG | $5^{th}$ order Low pass | 5 |
| VPG | $5^{th}$ order Bandpass | [0.5,18] |
| APG | $5^{th}$ order Bandpass | [0.5,30] |

The low-pass filters applied to the ECG and PPG signals are to remove high-frequency noise above 5 Hz. After preprocessing, the 1-minute data from all signals were then selected from the original 3-minute recordings based on the criteria of consistency of waveforms and detectability of basic features (P-QRS-T for ECG, peaks, troughs and dicrotic notch for PPG).

Using the normalized ECG and PPG time-synchronized signals, the PAT was then acquired (Figure 6). One-minute durations of data were selected for each subject to avoid repetitive waveforms causing additional computational costs during extraction of the features of each waveform.

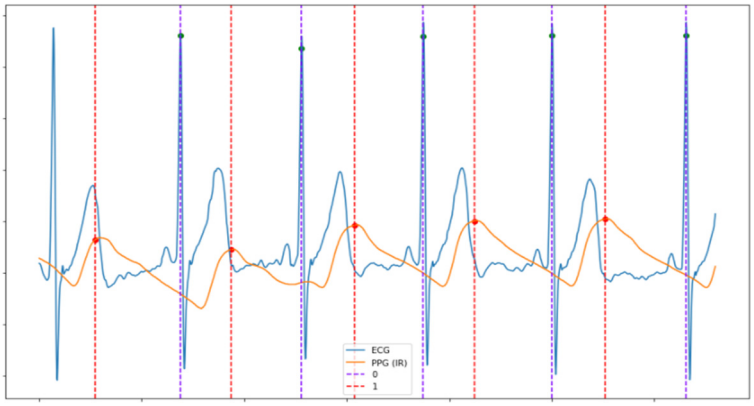


**Figure 6.** Detected ECG QRS peaks denoted by blue dotted lines and PPG pulse peaks denoted by red dotted lines; the signal acquisition time has been synchronized; the distance between the blue and red dotted lines is the PAT.

### 2.3.1. PPG morphological features

Numerous studies have proposed many different combinations from more than 107 PPG morphological features [10,31,32]. Before extracting these features, each PPG signal was tagged with some of the basic features. The annotation of labels was done automatically based on the represented parameters of the PPG signal. Only four main essential features of the PPG waveform were required and extracted for a section of the algorithm. They included the systolic peak, trough, dicrotic notch and diastolic peak. Figure 7 shows systolic peaks, diastolic peaks, dicrotic notches and troughs that were located for each waveform and have been identified and labeled based on their reference to the neighboring feature. The features were obtained by using Python package HeartPy [46].

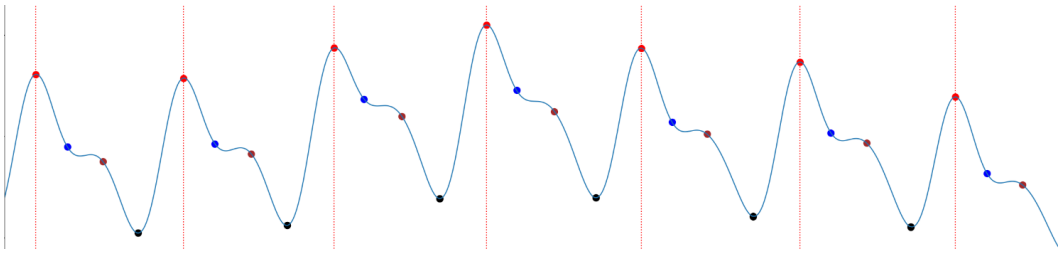

**Figure 7.** Labeled PPG. Red: Systolic peaks; Brown: Diastolic peaks; Blue: Dicrotic notch, Black: Pulse foot troughs.

The features included the frequency and time domains, statistical and demographic characteristics and features from the first and second derived PPG signals. The 45 features containing cardiovascular information that can be extracted for each cardiac cycle or waveform and then identified and divided into three parts: ECG-PPG time differences, heart rate variability (HRV) and PPG morphological features, and each of them is supported by physiological relevance. Each feature was then evaluated for its physiological association with BP, and, finally, 24 features were selected as input to the proposed machine learning models [28].

Numerous features can be extracted from the labeled PPG data, but too many features as input to machine learning models will not produce more accurate results. Instead, overfitting is likely to occur, i.e., the model learns too much detail and variation in the training data and is therefore less amenable to fitting an additional dataset, resulting in poor model performance. Using the data shown in Figure 7, we further processed the waveform to generate Figure 8 as a spatially layered labeled PPG plot with black dots labeling the pulse start and end troughs, red dots for the systolic peaks, brown dots for the diastolic peaks and blue dots for the dicrotic notches. The pulse duration variability can be clearly seen for each pulse wavelet when the starting pulse foot is pinned at $t = 0$. This process is important when using each ECG-PPG data window to acquire the PAT.

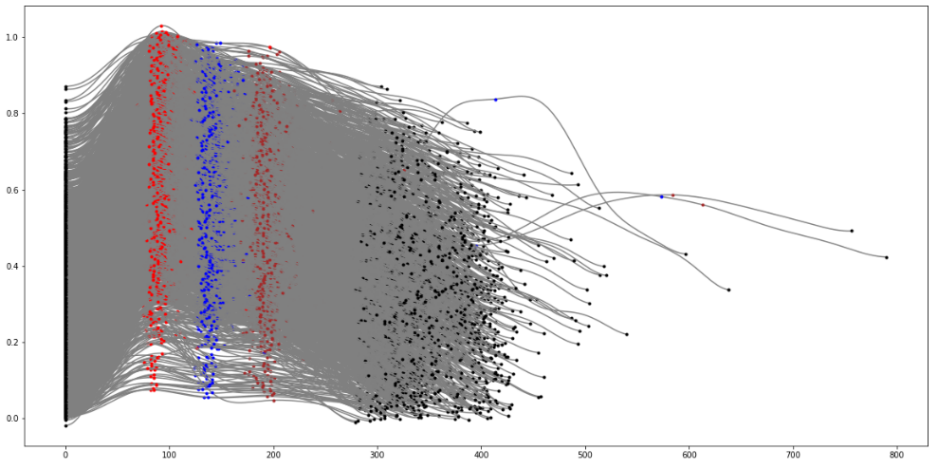


**Figure 8.** Labeled PPG data that have been normalized and pulse-foot pinned to $t = 0$ for a single individual; the labeled systolic peaks are in red, the dicrotic notches are in blue, the diastolic peaks are in brown and the pulse troughs are denoted by black points.

Past studies suggested feature-ranking methods, including manually selecting PPG morphological features using physiological theory [47], statistical analysis methods such as variance selection [48] and the use of simple machine learning models such as random forest (RF) and k-nearest neighbor models [29,31]. Ten morphological PPG features were selected by applying a feature-ranking method.

We applied theoretical analysis by selecting the simpler and more accurately detected features, because the waveforms were not perfect and more complex features would potentially affect robustness. In addition, feature-identification methods involving machine learning algorithms could lead to unexplained results, such as RF feature selection, which tends to select uninformative features for node partitioning [49].

### 2.3.2. VPG and APG morphological features

VPG is the 1st derivative of PPG, and the 2nd derivative of PPG is known as the APG [10]. For detection of the systolic peaks and troughs of PPG signals, the gradients or slopes of the 1st-derivative PPG whenever it intersects the point (y = 0) were located as shown in Figure 9A. At the intersection point, a positive gradient or increasing slope suggests a positive change in the direction of the PPG wave, while a negative gradient or decreasing slope implies a negative change in the direction of the PPG wave. Thereafter, the steepness of the change in direction can be obtained from the magnitude of the gradients.

For VPG data, four characteristic points have been proposed [50], as can be seen in the single VPG waveform in Figure 9B. However, since the self-collected PPG signals had imperfect waveforms, one feature, namely, the first local minima (x), was not observable in each waveform. Therefore, only three features were selected in a single VPG waveform, namely, the global maxima (w), global minima (y) and local maxima after the global minima (z).

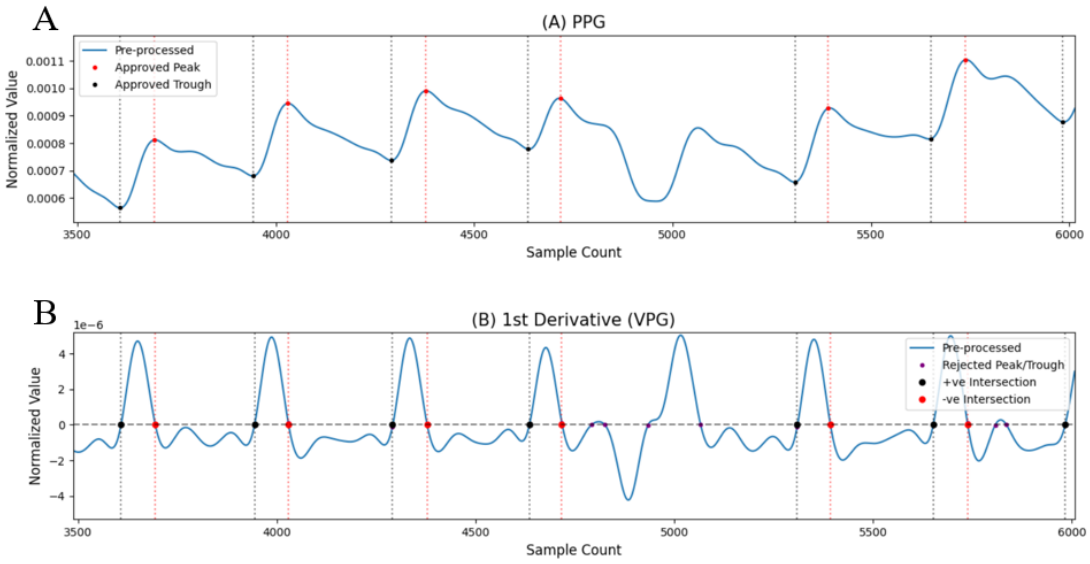


**Figure 9.** A: 0th-order PPG data were first analyzed for the detection of PPG peaks (systolic peaks) and troughs. B: 1st derivative of the PPG; a VPG waveform showing accepted and rejected intersection points from the 1st derivative of the PPG waveform.

By identifying the steepness of the changes in direction of the PPG waves, the systolic peaks and troughs were easily extracted where the points were only accepted if they were either less than the mean negative gradient or greater than the mean positive gradient for systolic peaks and troughs, respectively. Otherwise, the wavelets were rejected due to low gradient steepness.

For APG data, five characteristic points were implemented: global maxima (a), global minima (b), local maxima (c), local minima (d) and the nearest local maxima after d (e). These features are similarly labeled in Figure 6 (left), but only a and b can be identified in all APG waveforms. Figure 10 represents the ECG, PPG, VPG and APG data with the identified feature points on the waveforms.

The final selected PPG morphological features are included in Table 4, along with all other features, with a brief description for each. From an individual's 1-minute PPG data, the first three waveforms were selected for feature extraction and the average of these waveforms was used as input to machine learning. It was assumed that, after manual selection of the 1-minute waveforms, as described in Section 2.2, the first three individual waveforms in each 1-minute PPG recording would be consistent and sufficient to represent the person's entire PPG data span.

Because fewer traits were selected in this study than in many other studies based on the remaining VPG and APG traits, the performance of the machine learning models differed. However, by using only features that were uniquely and accurately detected on each waveform (w, y, z for VPG and a, b for APG), the robustness of the machine learning models was increased [31], and this was in line with the aim of this work, which was to increase the robustness of BP estimation under real-world conditions.

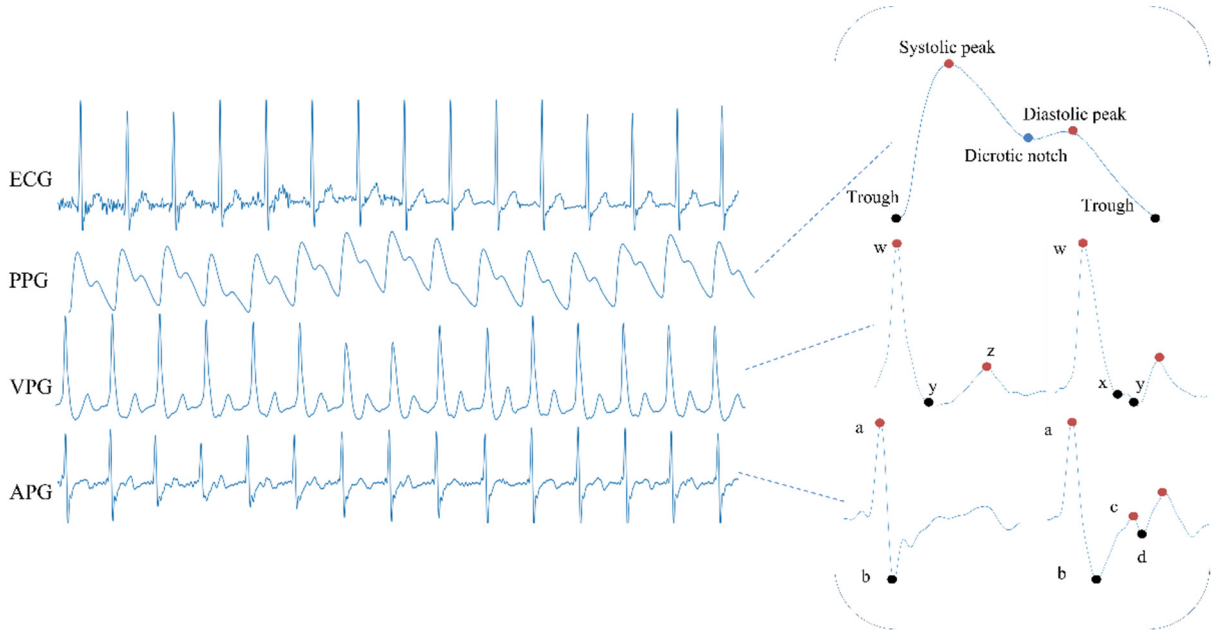


**Figure 10.** VPG and APG waveforms. VPG waveform with w, x, y and z all observable (left), and VPG waveform with only w, y and z observable. APG waveform with a, b, c, d and e all observable, and APG waveform with only a and b observable.

**Table 4.** Final feature set with 24 features.

| Features | Definitions |
|---|---|
| PAT | Time difference between the peak of the ECG R wave and PPG systolic peak |
| SDNN | HRV subset; standard deviation of the PPG peak-to-peak (PP) intervals |
| RMSSD | HRV subset; root mean square of the successive differences (RMSSD) |
| BPM | Heart beats per minute |
| Systolic Peak Amplitude | Amplitude of systolic peak of PPG waveform |
| Diastolic Peak Amplitude | Amplitude of diastolic peak of PPG waveform |
| Dicrotic Notch Amplitude | Amplitude of dicrotic notch of PPG waveform |
| Pulse Interval | Time difference between two PPG waveforms |
| Augmentation Index | Ratio of diastolic peak amplitude to the corresponding systolic peak amplitude |
| Systolic Peak Time | Time difference between the start and the systolic peak of a single PPG waveform |
| Diastolic Peak Time | Time difference between the start and the diastolic peak of a single PPG waveform |
| Dicrotic Notch Time | Time difference between the start and the dicrotic notch of a single PPG waveform |
| Time Between Systolic and Diastolic Peaks | Time difference between the systolic peak and diastolic peak of a single PPG waveform |
| w | Global maxima of VPG waveform |
| Time to w | Time difference between the start and w of a single VPG waveform |
| y | Global minima of VPG waveform |
| Time to y | Time difference between the start and y of a single VPG waveform |
| z | Local maxima of VPG waveform after y |
| Time to z | Time difference between the start and z of a single VPG waveform |
| a | Global maxima of APG waveform |
| Time to a | Time difference between the start and a of a single APG waveform |
| b | Global minima of APG waveform |
| Time to b | Time difference between the start and b of a single APG waveform |
| b/a | Ratio of b to the corresponding a |

#### 2.3.3. HRV and PAT

It is worth mentioning that, many studies used only the PAT [17] or only PPG morphological features [28,51,52]; however, we propose a feature set with three main categories: PAT, HRV features and PPG morphological features. The reason for having more categories of features instead of having more features in one category is that they each reflect different information [47], and we wanted to avoid overfitting.

The heart rate refers to the number of times the heart beats within a minute, while the changes in the time intervals between each successive heartbeat is HRV [53]. HRV is typically used for evaluation of general cardiac health, as well as the condition of the autonomic nervous system. It provides useful insight into the sympathetic-parasympathetic autonomic balance and, therefore, the potential risk of cardiovascular conditions.

The remaining two parameters included in the feature set are HRV and the PAT components. In this case, a beat-to-beat time measurement was required for HRV (beat to beat between each R-R ECG peak) and the PAT (beat to beat between each ECG-PPG R-P peak).

The RR interval (RRI) was derived from the intervals between peaks of two successive R waves of the QRS complex from the ECG, while the peak-peak interval (PPI) was derived from the intervals between two successive peaks of each PPG waveform [54,55]. Incidentally, the RRI is sometimes referred to as N-N intervals, which is derived from "normal" R peaks. Figure 11 represents how HRV can be extracted from ECG and PPG data respectively referred to as "RR-interval" and "PP-interval".

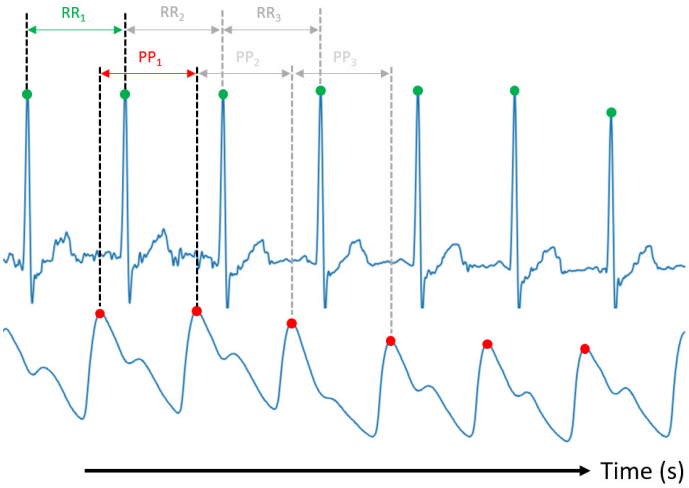


**Figure 11.** RR interval and PP interval.

We acquired the PAT of each ECG-PPG pulse (see Figure 12), and each PAT value is now a contributing parameter to the input feature set. As discussed in Section 1.1, the PAT component alone is insufficient due to the PEP [25]; thus, HRV-related parameters are correlated with hypertension, such as the standard deviation of the interbeat intervals (SDNN) and RMSSD, which were found to be significantly lower in hypertensive individuals [56,57]. As such, the parameters SDNN and RMSSD were included in the feature set, as suggested by past research [56], to show the most significant change in the hypertensive subjects relative to the normotensive subjects and thus mitigate the PAT as a sole major component in BP estimation.

Interestingly, both the HRV and PAT yielded very similar time-series morphologies and appeared to have similar variances due to the nature of the parameters. However, because HRV represents the electrical function of the heart and PAT includes the hemomechanical components of pulsatile blood flow in the extremities, the two values are not directly comparable, and were therefore used as two different input characteristics.

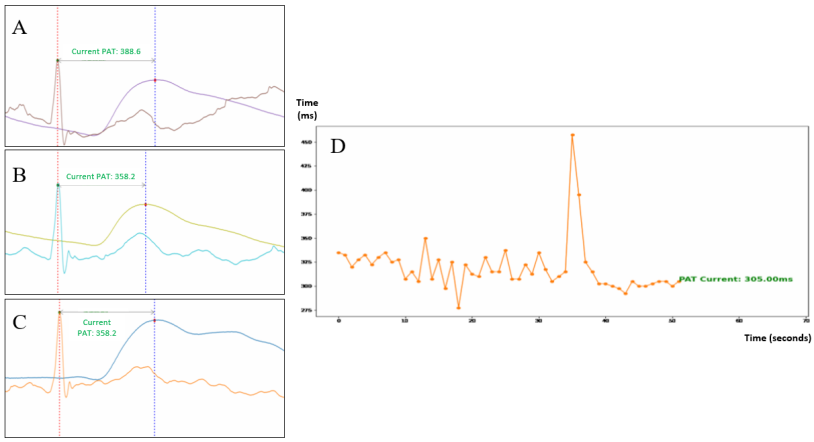


**Figure 12.** Labels A to C show three wavelets in a window of three consecutive heartbeats, showing our method to capture successive beat-to-beat PAT values for three ECG-PPG pulses. D: Plots of the PAT values over time for a specific subject's data capture duration.

### *2.4. Machine learning processing*

Previous work on BP estimation based on ECG-PPG data have also shown much promise, as is evidenced by the use of RF regression (RFR) [56], support vector machines [57,58], Adaboost regression (Adaboost-R) [16,58] and repetitive neural networks [43].

A standard train/test split of 80/20 approach was applied to the collected data randomly to train the machine learnings under study and balance the challenges of parameter variance versus variance in predicted estimation performance. Because the collected dataset was small, we performed cross-validation by randomly selecting a subset of the entire dataset in an 80/20 training/testing profile and determining the performance on each validation set.

That is, a training set was applied to Subjects #1, #5, #8, #9... (44 data points) to train each identified machine learning model for RFR, SVR, Adaboost-R and ANNs, and the remaining 10 data points were then used to test the predictive performance of the trained dataset. In the next run, Subjects #1, #3, #6, #10, #11 (44 data points) were randomly trained. This was then repeated over a series of runs to determine that the variances in parameters and predictive performance would be consistent regardless of the training or test dataset selected.

### *2.5. Ethics approval for research*

This research and related protocols were approved by the Institutional Review Board (NTU-IRB) of Nanyang Technological University (IRB-2020-07-005; ERMP amendment-Ver 18.0). Project Title: Investigate the feasibility of non-invasive PPG/ECG biosignals to estimate an individual's BP/BGL values. All participants provided written informed consent prior to data collection as part of the study.

## 3. Results

As discussed in Section 1.2 on the Limitations of machine learning/deep learnings on ECG-PPG

approaches, we chose to avoid recent deep learning methods, and instead chose machine learning models that have direct and linear explainability that could be expected to perform relatively well on a small dataset.

After establishing the parameters and characteristics of the ECG-PPG data for training, as mentioned in the previous section, we identified and implemented four models: RFR, SVR, Adaboost-R and ANN. Each regression model was evaluated by using the performance metrics MAE and root mean square error (RMSE). The MAE is the average magnitude of the difference between the predicted outcome and the actual measurement, and the RMSE is the square root of the root mean square error. The performance of each of the four proposed machine learning models is shown in Figure 13.

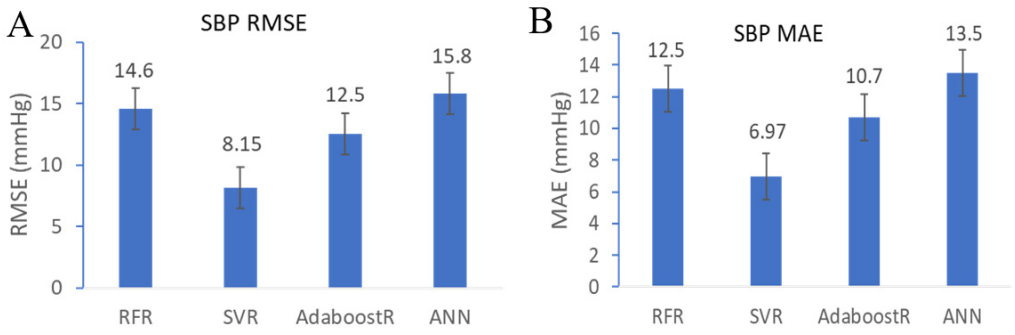


**Figure 13.** A: RMSE between measured SBP and predicted SBP for each of the four investigated machine learning models; error bars represent standard deviation. B: MAE between measured SBP and predicted SBP for each of the four machine learning models. RMSE and MAE show that SVR had superior performance of the four.

The results suggests that SVR was the best performing model in terms of MAE and RMSE, achieving an SBP MAE of 6.97 and RMSE of 8.15, while the ANN model was the worst performing model, with an MAE of 13.5 and RMSE of 15.8; the ranking of models according to the MAE matched that for the RMSE (ranking from the best- to the worst-performing model: SVR, AdaboostR, RFR, ANN). The obtained MAE can be compared with the British Hypertension Society (BHS) grading criteria [4,59].

By comparing the MAE results to the BHS grading criteria, as shown in Figure 13 and Table 5, only SVR matched the recommended grade of C, while others fell into a grade of D. As a reference to the final goal of implementing the algorithms on a wearable device, it must achieve a grade of at least B for SBP [60].

The mean rank for all 54 subjects was then calculated and obtained for the BP. For the SBP, the obtained p-value for all mean errors was 0.005207; therefore, the null hypothesis was rejected at $\alpha = 0.05$. For the diastolic condition, the p-value obtained for all mean error values was 0.3273; thus, the null hypothesis was not rejected at $\alpha = 0.05$. Both the SBP and DBP estimation from our method with SVR appeared to be within ±15 mmHg of the actual BP measured by a traditional Omron HEM-7600T brachial sphygmomanometer. The results are promising and shed light in the direction of non-occlusive continuous BP estimation. Figure 14 shows the estimated BP from the SVR-trained model versus the actual BP with errors consistent when BP is at the extreme values (lower and upper value).

**Table 5.** Grading criteria used by the BHS summarized into MAE and the corresponding grades.

| MAE (mmHg) | BHS | Recommended Grade |
|---|---|---|
| <4 | Grade A | A |
| 4–5 | Mostly Grade A, less in Grade B | A |
| 5–6 | Mostly in Grade B, less in Grade A, extremely less in Grade C and Grade D | B |
| 6–7 | Mostly in Grade C, less in Grade B and Grade D | C |
| 7 | Worse than Grade C | D (unacceptable) |

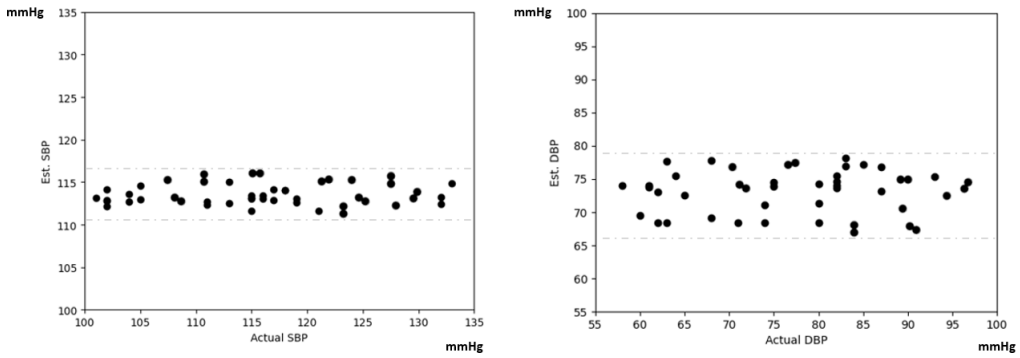


**Figure 14.** Performance of our SVR BP estimation model in comparison with the reference SBP (left) and DBP (right). Measured BP plotted against estimated BP for the test set; SBP and DBP show high linearity for the population tested.

## 4. Discussion

SVR uses a nonlinear mapping method to map the input features to a higher dimensional space using a kernel function. The kernel used here was the radial basis function. The main advantage of SVR is that it can model nonlinear relationships well. Given a large number of PPG morphological features that have nonlinear relationships with SBP, this model showed the best result in BP estimation (systolic).

In this work, the RFR model was implemented with 100 trees and a maximum depth of five trees, but there is a difficult trade-off between training time (and space) and a larger number of trees. A larger number of trees can improve the accuracy of the prediction but increase the computational cost. If the number of weakly learning trees is too small, underfitting can easily occur; but, if it is too large, computational costs increase with diminishing returns. In addition, RFR may overfit on data with a lot of noise. Decision trees tend to overfit in prediction. RFs reduce the degree of overfitting by tuning, but their prediction is still subject to more overfitting than a linear model. On the other hand, Adaboost-R is another popular ensemble method based on many decision trees (weak estimators); but, in Adaboost-R, weights are applied to the results of these decision trees. The weights vary so that the algorithm focuses on the training samples that are more difficult to estimate in the training process.

ANNs constitute the only model that uses neural networks. Here, only a hidden layer was built for the neural networks to reduce the complexity. Neural networks are best able to handle complex tasks, especially when the dataset is large. Due to its iterative learning process for the relationship

between features and SBP, ANNs are suitable for dealing with nonlinear relationships when estimating BP. However, as expected, the ANN model performed the worst due to the small dataset, a well-known weakness of neural network methods.

Of the four proposed models, only SVR met the Grade C BHS criteria, while the remaining models were not acceptable. This suggests that there are limitations in the methodology and dataset, as many other studies have reported a MAE of less than 3 mmHg [61].

A drawback of using our self-collected dataset is that the data were not divided into different age groups due to the small number of subjects, although age has been suggested as an important factor in PPG morphology, especially for the dicrotic notch and inflection point due to lower arterial elasticity in the elderly [62].

In feature selection, the contribution of each category (PAT, HRV, PPG morphology) to machine learning remained unknown. Further feature selection techniques can be explored to remove less informative features. Because there is a trade-off between explainability and informativeness in the selection of machine learning/deep learning as model complexity increases, this work did not determine the extent to which model complexity should increase, which may be the cause of the less desirable results.

## 5. Conclusions

In this study, a self-sampled dataset containing ECG, PPG and BP data was analyzed, along with 24 multivariate-derived trait parameters identified as input parameters for the four specific machine learning methods (i.e., RFR, SVR, Adaboost-R and ANN). Performance evaluation of the four machine learning methods in our study shows that SVR performs best for BP estimation with noisy data, achieving an MAE of 6.97 mmHg, which meets the BHS Grade C criteria.

We demonstrated that ambulatory ECG-PPG signals collected from mobile discrete devices can be used to estimate BP under real-world conditions and discussed the theory of why, of the four machine learning models compared and evaluated, SVR emerged as the best-performing model; it is likely due to the algorithm's ability to handle the nonlinear relationship between features and BP.

Because there is a trade-off between explainability and performance in the selection of machine learning/deep learning models with increasing model complexity, this work did not determine the extent to which model complexity should increase, which could be the cause of the less desirable results in other models. Previous work using "black box" deep learning approaches could potentially introduce FDA compliance issues.

For ECG-PPG to be practical and economical for use in a wearable for monitoring BP, further research is needed to achieve an optimal balance between computational cost (limited battery power), explainability and prediction/estimation accuracy. Only when an appropriate balance or hybrid technique is achieved between the machine learning and deep learning approaches that can be applied to noisy, corrupted biosignals will non-occluding BP measurement devices become practical and reliable enough for clinical implementation.

For feature selection, the contribution (e.g., Pareto analysis) of each category (i.e., PAT, HRV, PPG morphology) to machine learning is still unknown and could be part of further feature-selection procedures to remove less informative features and optimize computational costs.

The authors will try to include a larger number of participants in a larger study to improve the receiver operating characteristic of the BP estimation model. With a larger dataset, we can attempt to benchmark our method against deep learning methods described by other authors that do not use a

smaller dataset. Benchmarking will be a goal of future work.

**Acknowledgments**

The authors gratefully acknowledge the support of the Institute for Health Innovation & Technology (iHealthtech). This work was funded by the Singapore Health Technologies Consortium (HealthTEC) (Grant No: HealthTec 2/2020-6). The authors have confirmed that all identifiable participants in this study have given consent for publication. The authors also thank the anonymous volunteers who participated in data collection.

**Conflict of Interest**

The authors declare that there is no conflict of interest.

**References**

1. P. M. Kearney, M. Whelton, K. Reynolds, P. Muntner, P. K Whelton, J. He, Global burden of hypertension: analysis of worldwide data, *lancet*, **365** (2005), 217–223. https://doi.org/10.1016/S0140-6736(05)17741-1
2. G. A. Roth, M. H. Forouzanfar, A. E. Moran, R. Barber, G. Nguyen, V. L. Feigin, et al., Demographic and epidemiologic drivers of global cardiovascular mortality, *N. Engl. J. Med.*, **372** (2015), 1333–1341. https://doi.org/10.1056/NEJMoa1406656
3. K. T. Mills, A. Stefanescu, J. He, The global epidemiology of hypertension, *Nat. Rev. Nephrol.*, **16** (2020), 223–237. https://doi.org/10.1038/s41581-019-0244-2
4. B. Williams, N. R. Poulter, M. J. Brown, M. Davis, G. T. McInnes, J. F. Potter, et al., British Hypertension Society guidelines for hypertension management 2004 (BHS-IV): Summary, *BMJ*, **328** (2004), 634–640. https://doi.org/10.1136/bmj.328.7440.634
5. H. Y. Lee, T. Burkard, The advent of cuffless mobile device blood pressure measurement: Remaining challenges and pitfalls, *Korean Circ. J.*, (2022), **52** (3): 198–204. https://doi.org/10.4070/kcj.2021.0405
6. R. Mieloszyk, H. Twede, J. Lester, J. Wander, S. Basu, G. Cohn, et al., A comparison of wearable tonometry, photoplethysmography, and electrocardiography for cuffless measurement of blood pressure in an ambulatory setting, *IEEE J. Biomed. Health Inform.*, **26** (2022), 2864–2875. https://doi.org/10.1109/JBHI.2022.3153259
7. J. Esmaelpoor, Z. M. Sanat, M. H. Moradi, *Blood Pressure Monitoring Using Photoplethysmogram and Electrocardiogram Signals*, 1$^{st}$ edition, CRC Press, Florida, 2021.
8. M. S. Tanveer, M. K. Hasan, Cuffless blood pressure estimation from electrocardiogram and photoplethysmogram using waveform based ANN-LSTM network, *Biomed. Signal Proces.*, **51** (2019), 382–392. https://doi.org/10.1016/j.bspc.2019.02.028
9. M. Hosanee, G. Chan, K. Welykholowa, R. Cooper, P. A. Kyriacou, D. Zheng, et al., Cuffless single-site photoplethysmography for blood pressure monitoring, *J. Clin. Med.*, **9** (2022), 723. https://doi.org/10.3390/jcm9030723
10. M. Elgendi, On the analysis of fingertip photoplethysmogram signals, *Curr. Cardiol. Rev.*, **8** (2012), 14–25. https://doi.org/10.2174/157340312801215782

11. E. Mejía-Mejía, J. Allen, K. Budidha, C. El-Hajj, P. A. Kyriacou, P. H. Charlton, 4-Photoplethysmography signal processing and synthesis, in *Photoplethysmography*, Academic Press, (2022), 69–146. https://doi.org/10.1016/B978-0-12-823374-0.00015-3
12. H. W. Loh, S. Xu, O. Faust, C. P. Ooi, P. D. Barua, S. Chakraborty, et al., Application of photoplethysmography signals for healthcare systems: An in-depth review, *Comput. Methods Programs Biomed.*, **216** (2022), 106677. https://doi.org/10.1016/j.cmpb.2022.106677
13. R. C. Block, M. Yavarimanesh, K. Natarajan, A. Carek, A. Mousavi, A. Chandrasekhar, et al., Conventional pulse transit times as markers of blood pressure changes in humans, *Sci. Rep.*, **10** (2020), 16373. https://doi.org/10.1038/s41598-020-73143-8
14. S. Heimark, O. M. H. Rindal, T. Seeberg, A. Stepanov, E. S. Boysen, C. L. Søraas, et al., Pulse arrival time can track changes in systolic blood pressure, *J. Hypertens.*, **39** (2021), e132. https://doi.org/10.1097/01.hjh.0000745808.43316.c3
15. E. Finnegan, S. Davidson, M. Harford, J. Jorge, P. Watkinson, D. Young, et al., Pulse arrival time as a surrogate of blood pressure, *Sci. Rep.*, **11** (2021), 22767. https://doi.org/10.1038/s41598-021-01358-4
16. L. P. Yao, Z. l. Pan, Cuff-less blood pressure estimation from photoplethysmography signal and electrocardiogram, *Phys. Eng. Sci. Med.*, **44** (2021), 397–408. https://doi.org/10.1007/s13246-021-00989-1
17. J, Lee, S. Yang, S. Lee, H. C. Kim, Analysis of pulse arrival time as an indicator of blood pressure in a large surgical biosignal database: Recommendations for developing ubiquitous blood pressure monitoring methods, *J. Clin. Med.*, **8** (2019), 1773. https://doi.org/10.3390/jcm8111773
18. M. Puig-de-Morales-Marinkovic, K. T. Turner, J. P. Butler, J. J. Fredberg, S. Suresh, Viscoelasticity of the human red blood cell, *Am. J. Physiol. Cell Physiol.*, **293** (2007), 597–605. https://doi.org/10.1152/ajpcell.00562.2006
19. M. Nichelatti, P. Pettazzoni, G. Pallotti, The study of viscoelastic behavior of blood vessels, *Blood Heart Circulation*, **1** (2017), 1–3. https://doi.org/10.15761/BHC.1000110
20. Z. Wang, M. J. Golob, N. Chesler, Viscoelastic properties of cardiovascular tissues, *Viscoelastic Viscoplast. Mater.*, **2** (2016), 64. https://doi.org/10.5772/64169
21. R. Raghu, I. E. Vignon-Clementel, C. A. Figueroa, C. A. Taylor, Comparative study of viscoelastic arterial wall models in nonlinear one-dimensional finite element simulations of blood flow, *J. Biomech. Eng.*, **133** (2011), 081003. https://doi.org/10.1115/1.4004532
22. D. H. Bergel, The dynamic elastic properties of the arterial wall, *J. Physiol.*, **156** (1961), 458–469. https://doi.org/10.1113/jphysiol.1961.sp006687
23. D. B. Camasão, D. Mantovani, The mechanical characterization of blood vessels and their substitutes in the continuous quest for physiological-relevant performances. A critical review, *Mater. Today Bio.*, **10** (2021), 100106. https://doi.org/10.1016/j.mtbio.2021.100106
24. S. Hodis, M. Zamir, Mechanical events within the arterial wall under the forces of pulsatile flow: A review, *J. Mech. Behav. Biomed. Mater.*, **4** (2011), 1595–1602. https://doi.org/10.1016/j.jmbbm.2011.01.005
25. S. L-O. Martin, A. M. Carek, C-S. Kim, H. Ashouri, O. T. Inan, J-O Hahn, et al., Weighing scale-based pulse transit time is a superior marker of blood pressure than conventional pulse arrival time. *Sci. Rep.*, **8 (**2018), 15838. https://doi.org/10.1038/srep39273
26. R. Barbieri, E. P. Scilingo, G. Valenza, *Complexity and nonlinearity in cardiovascular signals*, Springer, Berlin, 2017.

27. S. G. Khalid, J. Zhang, F. Chen, D. Zheng, Blood pressure estimation using photoplethysmography only: comparison between different machine learning approaches. *J. Healthc. Eng.*, (2018), 1548647. https://doi.org/10.1155/2018/1548647
28. M. H. Chowdhury, M. N. I. Shuzan, M. E. H. Chowdhury, Z. B. Mahbub, M. M. Uddin, A. Khandakar, et al., Estimating blood pressure from the photoplethysmogram signal and demographic features using machine learning techniques, *Sensors*, **20** (2020), 3127. https://doi.org/10.3390/s20113127
29. A. Chakraborty, D. Sadhukhan, S. Pal, M. Mitra, PPG-based automated estimation of blood pressure using patient-specific neural network modeling, *J. Mech. Med. Biol*., **20** (2020), 2050037. https://doi.org/10.1142/S0219519420500372
30. A. S. Zadi, R. Alex, R. Zhang, D. E. Watenpaugh, K. Behbehani, Arterial blood pressure feature estimation using photoplethysmography, *Comput. Biol. Med.*, **102** (2018), 104–111. https://doi.org/ 10.1016/j.compbiomed.2018.09.013
31. Z. Liu, B. Zhou, Y. Li, M. Tang, F. Miao, Continuous blood pressure estimation from electrocardiogram and photoplethysmogram during arrhythmias, *Front. Physiol*., **11** (2020), 575407. https://doi.org/10.3389/fphys.2020.575407
32. C. Sideris, H. Kalantarian, E. Nemati, M. Sarrafzadeh, Building continuous arterial blood pressure prediction models using recurrent networks, in *2016 IEEE International Conference on Smart Computing (SMARTCOMP)*, (2016), 1–5. https://doi.org/10.1109/SMARTCOMP.2016.7501681
33. H. Eom, D. Lee, S. Han, Y. S. Hariyani, Y. Lim, I. Sohn, et al., End-to-end deep learning architecture for continuous blood pressure estimation using attention mechanism, *Sensors*, **20** (2020), 2338. https://doi.org/10.3390/s20082338
34. A. Paviglianiti, V. Randazzo, S. Villata, G. Cirrincione, E. Pasero, A comparison of deep learning techniques for arterial blood pressure prediction, *Cognit. Comput.*, **14 (**2021), 1689–1710. https://doi.org/10.1007/s12559-021-09910-0
35. Y. Li, L. N. Harfiya, K. Purwandari, Y. Lin, Real-time cuffless continuous blood pressure estimation using deep learning model, *Sensors*, **20** (2020), 5606. https://doi.org/10.3390/s20195606
36. C. El-Hajj, P. A. Kyriacou, A review of machine learning techniques in photoplethysmography for the non-invasive cuff-less measurement of blood pressure, *Biomed. Signal Proces.*, **58** (2020), 101870. https://doi.org/10.1016/j.bspc.2020.101870
37. A. Papaa, M. Mitalb, P. Pisanoa, M. D. Giudice, E-health and wellbeing monitoring using smart healthcare devices: An empirical investigation, *Technol. Forecast. Soc.*, **153** (2020), 119226. https://doi.org/10.1016/j.techfore.2018.02.018
38. S. H. Chuah, P. A. Rauschnabel, N. Krey, B. Nguyen, T. Ramayah, S. Lade, Wearable technologies: The role of usefulness and visibility in smartwatch adoption, *Compu. Hum. Behav.*, **65** (2016), 276–284. https://doi.org/10.1016/j.chb.2016.07.047
39. M. Saeed, M. Villarroel, A. T Reisner, G. Clifford, L. Lehman, G. Moody, et al., Multiparameter Intelligent Monitoring in Intensive Care II (MIMIC-II): A public-access intensive care unit database, *Crit. Care Med*., **39** (2011) 952–960. https://doi.org/10.1097/CCM.0b013e31820a92c6
40. A. L. Goldberger, L. A. Amaral, L. Glass, J. M. Hausdorff, P. C. Ivanov, R. G. Mark, et al., PhysioBank, PhysioToolkit, and PhysioNet: Components of a new research resource for complex physiologic signals, *circulation*, **101** (2000), 215–220. https://doi.org/10.1161/01.cir.101.23.e215

41. E. Martinez-Ríosa, L. Montesinosa, M. Alfaro-Poncea, L. Pecchia, A review of machine learning in hypertension detection and blood pressure estimation based on clinical and physiological data, *Biomed. Signal Proces.*, **68** (2021), 102813. https://doi.org/10.1016/j.bspc.2021.102813
42. D. U. Jeong, K. M. Lim, Combined deep CNN–LSTM network-based multitasking learning architecture for noninvasive continuous blood pressure estimation using difference in ECG-PPG features, *Sci. Rep.*, **11** (2021), 13539. https://doi.org/10.1038/s41598-021-92997-0
43. Ü. Şentürk, I. Yücedağ, K. Polat, Repetitive neural network (RNN) based blood pressure estimation using PPG and ECG signals, in *2018 2nd International Symposium on Multidisciplinary Studies and Innovative Technologies (ISMSIT)*, (2018), 1–4. https://doi.org/10.1109/ISMSIT.2018.8567071
44. I. Eşer, L. Khorshid, U. Y. Güneş, Y. Demir, The effect of different body positions on blood pressure, *J. Clin. Nurs.*, **16** (2007), 137–140. https://doi.org/10.1111/j.1365-2702.2005.01494.x
45. J. A. Sukor, S. J. Redmond, N. H. Lovell, Signal quality measures for pulse oximetry through waveform morphology analysis, *Physiol. Meas.*, **32** (2011), 369–384. https://doi.org/10.1088/0967-3334/32/3/008
46. Paul van, HeartPy-Python Heart Rate Analysis Toolkit, https://python-heart-rate-analysis-toolkit.readthedocs.io/en/latest/ (11-July-2022)
47. J. Cano, A. Quesada, F. Ravelli, R. Zangróniz, R. Alcaraz, J. J. Rieta, Novel photoplethysmographic and electrocardiographic features for enhanced detection of hypertensive individuals, in *2021 International Conference on e-Health and Bioengineering (EHB)*, (2021), 1–4. https://doi.org/10.1109/EHB52898.2021.9657546
48. S. Chen, Z. Ji, H. Wu, Y. Xu, A non-invasive continuous blood pressure estimation approach based on machine learning, *Sensors (Basel)*, **19** (2019), 2585. https://doi.org/10.3390/s19112585
49. T. T. Nguyen, J. Z. Huang, T. T. Nguyen, Unbiased feature selection in learning random forests for high-dimensional data, *Sci. World J.*, (2015), e471371. https://doi.org/10.1155/2015/471371
50. M. Elgendi, Y. Liang, R. Ward, Toward generating more diagnostic features from photoplethysmogram waveforms, *Diseases*, **6** (2018), 20. https://doi.org/10.3390/diseases6010020
51. J. Dey, A. Gaurav, V. N. Tiwari, InstaBP: Cuff-less blood pressure monitoring on smartphone using single PPG sensor, in *2018 40th Annual International Conference of the IEEE Engineering in Medicine and Biology Society (EMBC)*, (2018), 5002–5005. https://doi.org/10.1109/embc.2018.8513189
52. H. Tjahjadi, K. Ramli, H. Murfi, Noninvasive classification of blood pressure based on photoplethysmography signals using bidirectional long short-term memory and time-frequency analysis, *IEEE Access*, **8** (2020). https://doi.org/10.1109/ACCESS.2020.2968967
53. T. Vandenberk, J. Stans, C. Mortelmans, R. Van Haelst, G. V. Schelvergem, C. Pelckmans, et al., Clinical validation of heart rate apps: mixed-methods evaluation study, *JMIR Mhealth Uhealth*, **5** (2017), e129. https://doi.org/10.2196/mhealth.7254
54. P. A. Lanfranchi, V. K. Somers, Cardiovascular physiology: autonomic control in health and in sleep disorders, in *Principles and Practice of Sleep Medicine*, Elsevier, (2017), 142–154. https://doi.org/10.1016/B978-0-323-24288-2.00014-3
55. N. Selvaraj, A. Jaryal, J. Santhosh, K. K. Deepak, S. Anand, Assessment of heart rate variability derived from finger-tip photoplethysmography as compared to electrocardiography, *J. Med. Eng. Tech.*, **32** (2008), 479–484. https://doi.org/10.1080/03091900701781317

56. A. Tiloca, G. Pagana, D. Demarchi, A random tree based algorithm for blood pressure estimation, in *2020 IEEE MTT-S International Microwave Biomedical Conference (IMBioC)*, (2020), 1–4. https://doi.org/10.1109/IMBIoC47321.2020.9385038
57. Y. Zhang, Z. Feng, A SVM method for continuous blood pressure estimation from a PPG signal, in *Proceedings of the 9th International Conference on Machine Learning and Computing*, (2017), 128–132. https://doi.org/10.1145/3055635.3056634
58. M. Kachuee, M. M. Kiani, H. Mohammadzade, M. Shabany, Cuffless blood pressure estimation algorithms for continuous health-care monitoring, *IEEE Trans. Biomed. Eng.*, **64** (2017), 859–869. https://doi.org/10.1109/TBME.2016.2580904
59. E. O'Brien, J. Petrie, W. Littler, M. de Swiet, P. L. Padfield, K. O'Malley, et al., The british hypertension Society protocol for the evaluation of automated and semi-automated blood pressure measuring devices with special reference to ambulatory systems, *J. Hypertens.*, **8** (1990), 607–619. https://doi.org/10.1097/00004872-199007000-00004
60. E. O'Brien, B. Waeber, G. Parati, J. Staessen, M. G. Myers, Blood pressure measuring devices: Recommendations of the European society of hypertension, *BMJ*, **322** (2001), 531–536. https://doi.org/10.1136/bmj.322.7285.531
61. L. Wang, W. Zhou, Y. Xing, X. Zhou, A novel neural network model for blood pressure estimation using photoplethesmography without electrocardiogram, *J. Healthc. Eng.*, (2018), 1–9. https://doi.org/10.1155/2018/7804243
62. Q. Yousef, M. B. I. Reaz, M. A. M. Ali, The analysis of PPG morphology: investigating the effects of aging on arterial compliance, *Meas. Sci. Rev.*, **12** (2012), 266–271. https://doi.org/10.2478/v10048-012-0036-3



AIMS Press